Supplementary Information

Control on Electron Tunnelling by Fine Band Engineering upon Semiconductor Potential Barriers

*Yunhao Zhao, Chenyuan Cai, Yi Zhang, Xuebing Zhao, Yingqiang Xu, Chongyun Liang, Zhichuan Niu, Yi Shi and Renchao Che**

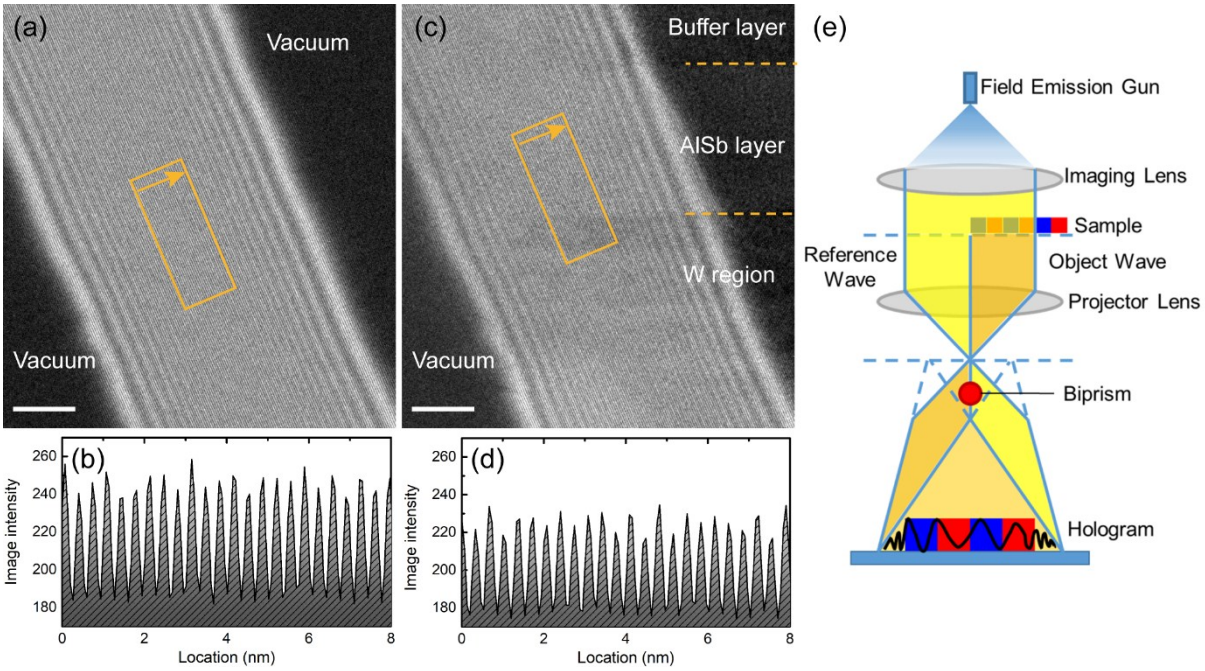

Fig. S1 Typical holograms and schematic diagram of off-axis electron holography. (a) and (c) Holograms with and without an inserted sample. The orange frames give the region of profiles below while the arrows show the direction. Different regions of the sample are indicated by dashed lines. (b) and (d) Profiles of image intensity of (a) and (c) respectively. (e) Optical mechanism of off-axis electron holography within TEM.

The holograms with and without an inserted sample are used together for reconstruction. Despite that image intensity for Fig. S1b is slightly weaker than Fig. S1a due to the sample inserting, fringes of both remain clear enough to provide effective electric information. From the sideband location (2.92 1/nm from the center) in the FFT image of the reference (not shown here), we can get a resolution of about 0.34 nm. The phase sensitivity of about 0.026 rad in this experiment could be obtained by $\Delta\varphi = \sqrt{2}/(V \times \sqrt{N})$, where V is the contrast of the hologram and N is the number of electron counts in each reconstructed pixel. The V of about 15% could be obtained from Fig. S1 while the N is nearly 500 during our experiments.

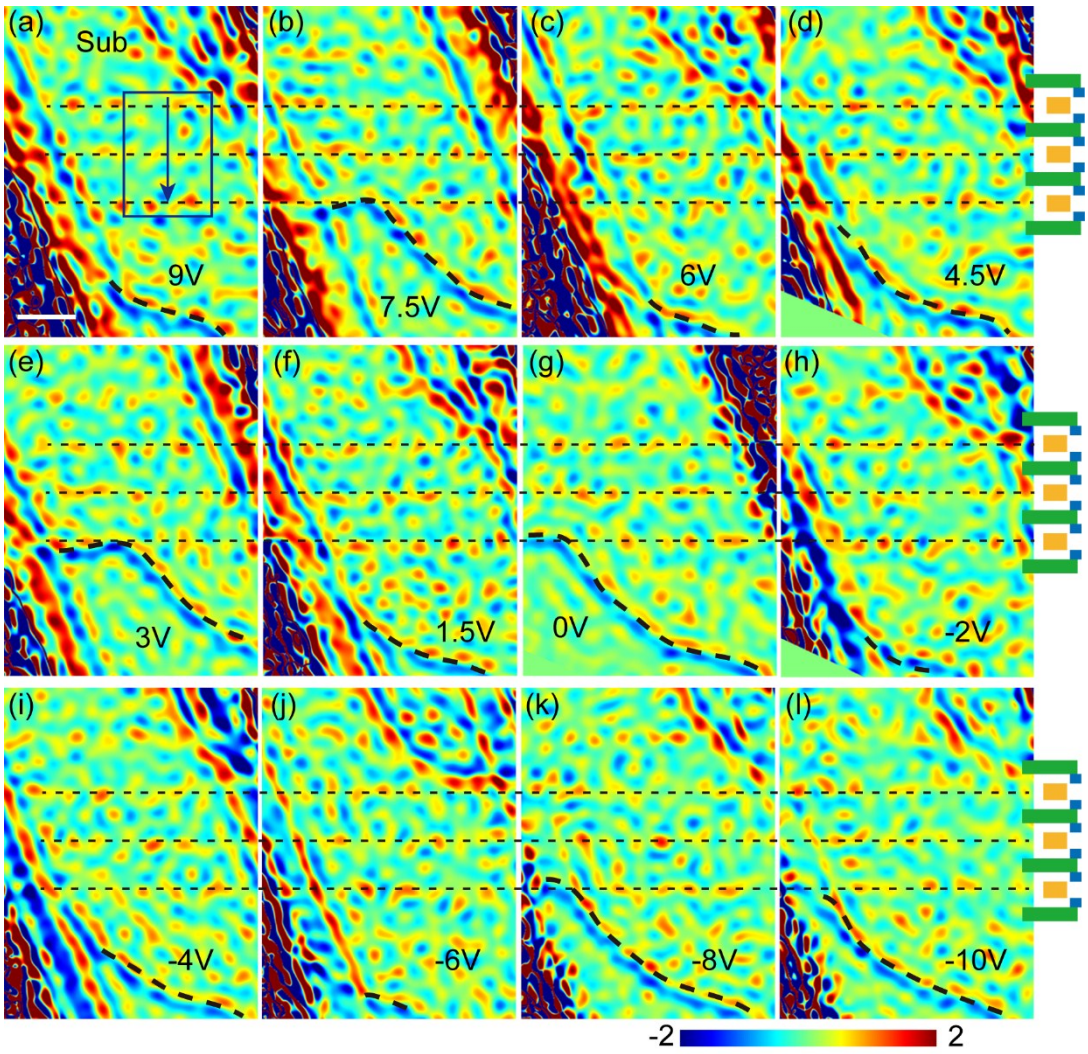

Fig. S2 Charge density distributions under series of voltages within "W" structure. (a)-(l) Charge density maps of 9V, 7.5V, 6V, 4.5V, 3V, 1.5V, 0V, -2V, -4V, -6V, -8V and -10V. The unit is e/nm^3. The black frame in (a) shows the region of the corresponding profile while the arrow gives the direction. The colored blocks on the right indicate energy band alignment for AlSb (green), InAs (blue) and InGaSb (yellow) while their locations are aligned with charge density maps by straight dashed lines. The margin of the sample is indicated by curved thick dashed lines.

According to the valance and conduction band offset between different materials, InGaSb and AlSb layers should serve as quantum wells for holes while electrons would accumulate mainly in InAs layers. All charge density maps in Fig. S2 confirm such deduction with negative signals in InAs and positive ones in InGaSb and AlSb. Note that although the locations of our sample seem different under different voltages in the images, all the locations aligned by straight dashed lines are the very same material layers.

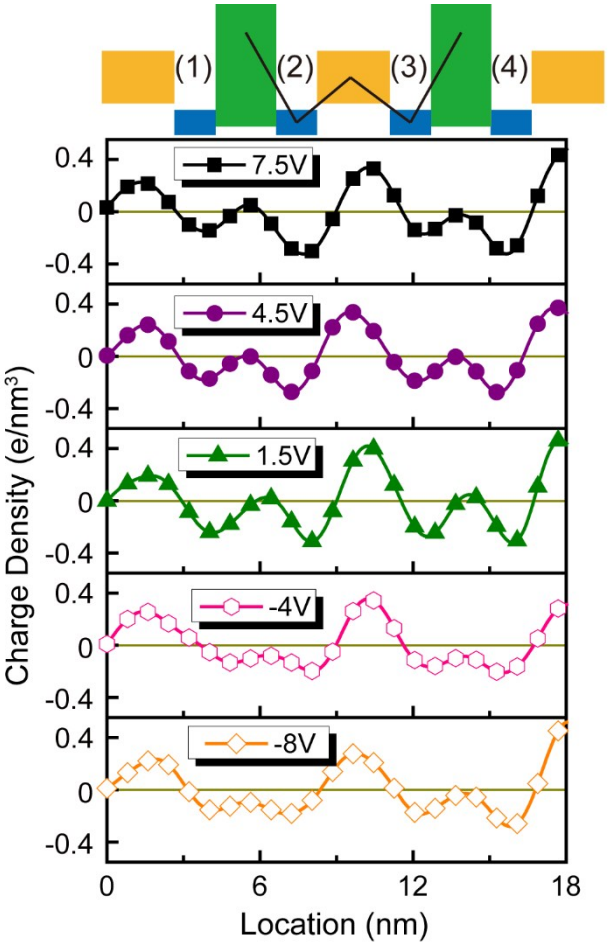

Fig. S3 Charge density profiles within the "W" region. Charge density profiles under positive (1.5V, 4.5V, 7.5V) and negative (-4V, -8V) voltages. Colored blocks indicate energy band alignment for AlSb (green), InAs (blue) and InGaSb (yellow) while their locations are aligned with lower curves.

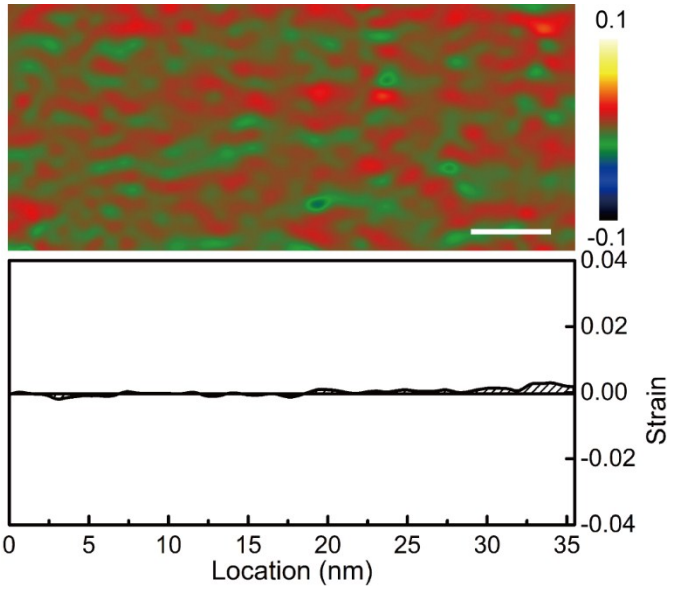

Fig. S4 Strain analysis by GPA. Strain distribution and the corresponding profile in the in-plane direction of Fig. S3a in the manuscript. The profile is averaged in the [110] direction as the same case with Fig. S3c. The scales are 10 nm.

Strain along the in-plane direction is only about ±0.1% and evenly distributed along the growth direction. Such weak strain means that the stress induced by lattice discrepancy has been totally relaxed during growth. Thus, defects such as dislocation won't be easily induced in our multilayer to remain good growth quality.

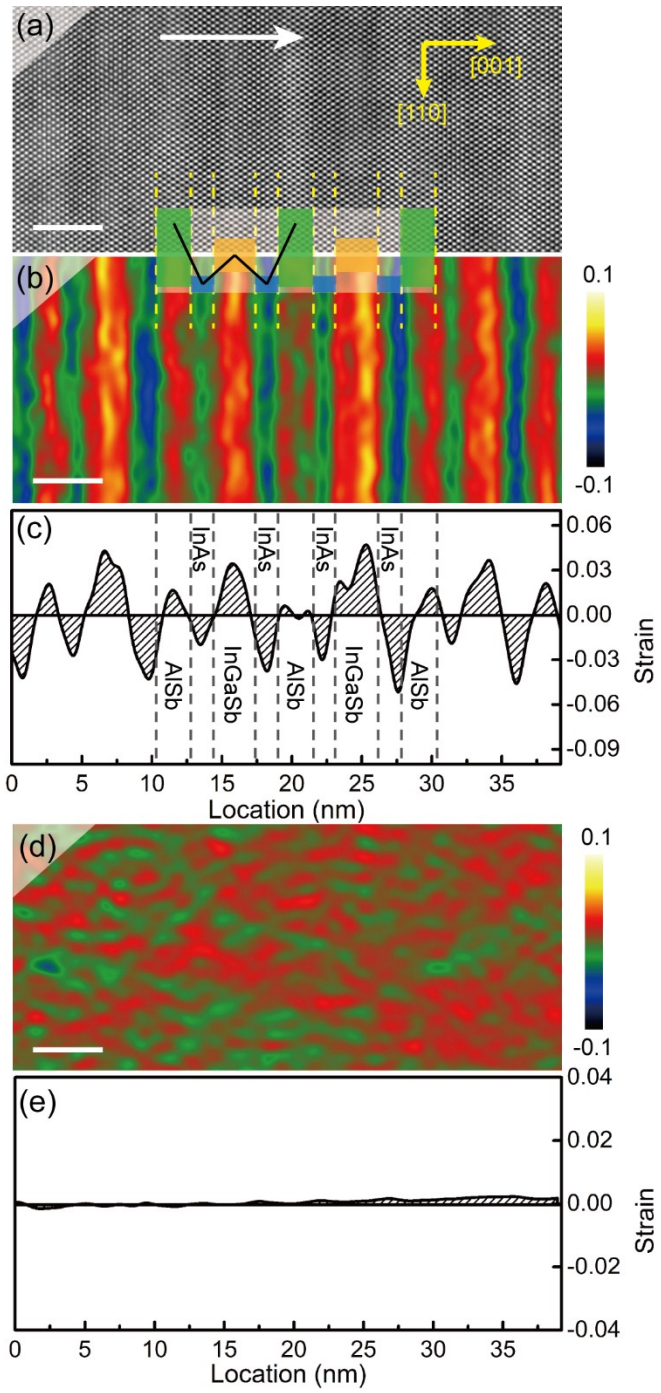

Fig. S5 Strain analysis by GPA within another area of the same sample. (a) High-resolution TEM image of several periods of "W" structure. The white arrow in the top show growth direction and yellow arrows give orientation index. (b) Strain distribution in growth direction within (a) and the color marker is on the right. Note that the reference is selected as the whole image in (a). Colored blocks between (a) and (b) indicate energy band alignment for AlSb (green), InAs (blue) and InGaSb (yellow) and their locations are aligned. (c) Strain profiles of (b) along the growth direction (averaged in the [110] direction). Materials are labeled and aligned with the above colored blocks. (d). Strain distribution in in-plane direction within (a) and the color marker is on the right. (e) Strain profiles of (d) along the growth direction (averaged in the [110] direction). The scales are 10 nm.

Strain in the in-plane direction is only about ±0.1% and evenly distributed along growth direction which indicates that the stress induced by lattice discrepancy has been totally relaxed during growth. Thus, the lattice difference of our materials should be reflected mainly in the strain distribution of [001] direction. Although the strain distribution is consistent with lattice sizes of AlSb (6.1355Å), InAs (6.0583Å), and In0.35Ga0.65Sb (6.2301Å), the low-left-high-right strain status within AlSb and InGaSb layers shows apparent unevenness. Meanwhile, the compressive strain of InAs layers grown on AlSb is relatively smaller than those grown on InGaSb. Such phenomena in Fig. S5 are similar to those in Fig. S3 and could be explained by several element behaviours mentioned in the manuscript.

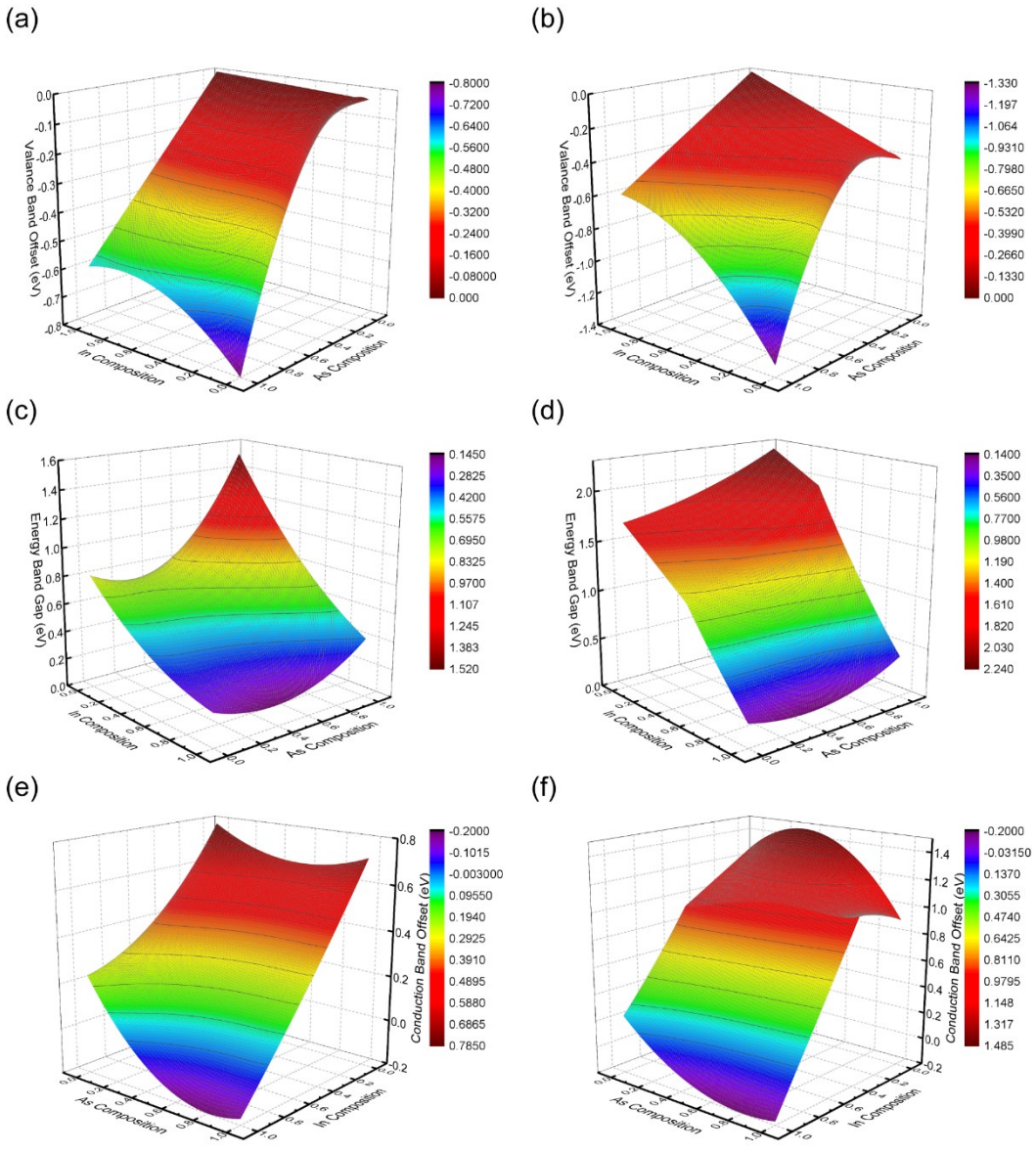

Fig. S6 Energy band parameters calculated based on interpolation formulas. (a) and (b) Valance band offsets (VBO) of quaternary alloy InGaAsSb and InAlAsSb respectively. (c) and (d) Minimal bandgap among Γ, X, and L of InGaAsSb and InAlAsSb respectively. (e) and (f) Conduction band offsets (CBO) of InGaAsSb and InAlAsSb respectively. Note that the VBO and CBO values are relative ones while the VBO of InSb is chosen as 0.

Results here are the approximated energy band parameters for quaternary alloys. Based on the compositional variation deduced from strain analysis, an energy band model could be established according to the parameters in Fig. S6. Meanwhile, such calculation based on interpolation formulas were used in simulations as default.

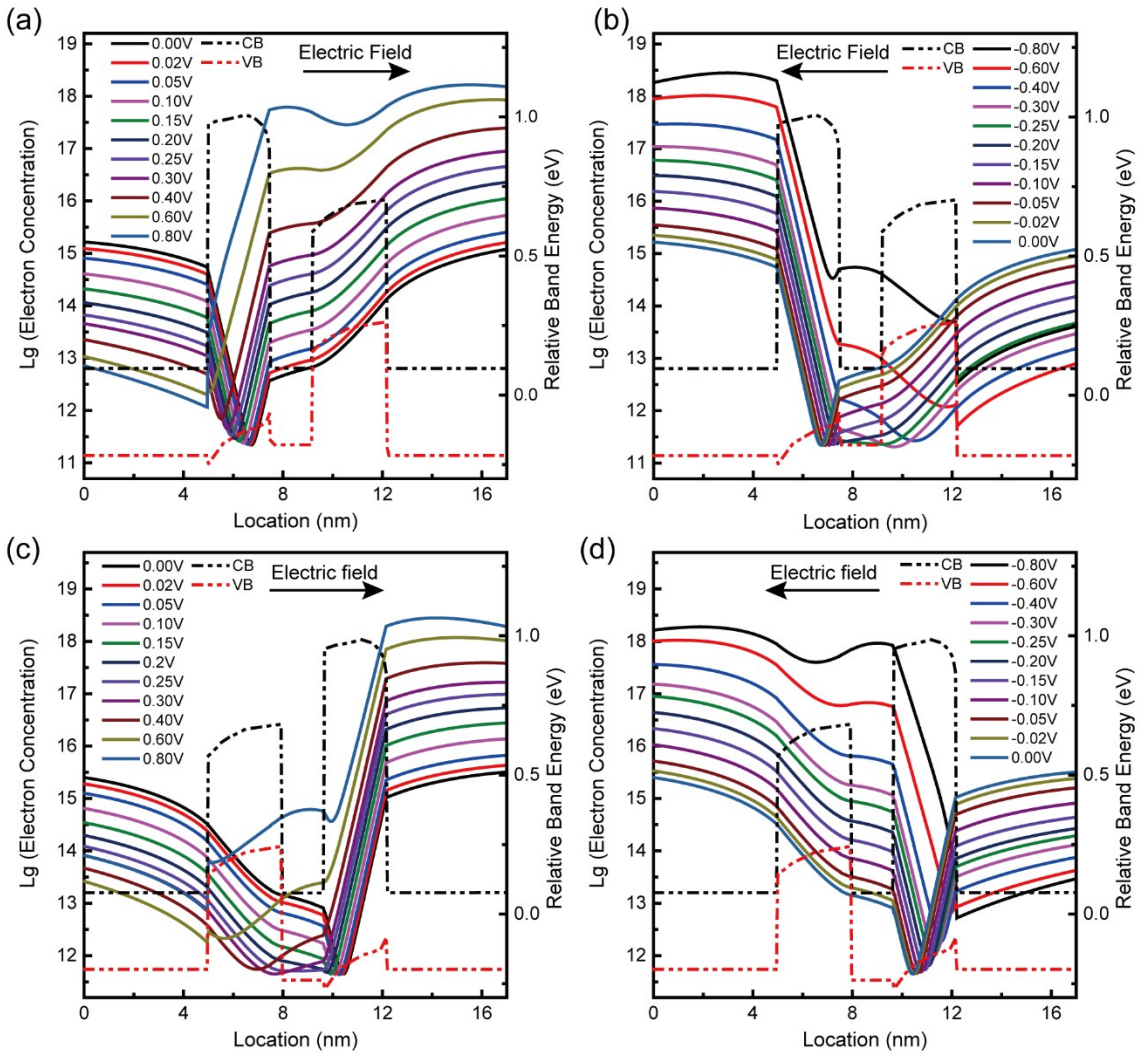

Fig. S7 Theoretical simulations on electron distribution within modified AlSb/InAs/InGaSb and InGaSb/InAs/AlSb structures. (a) and (b) Common logarithm of electron concentration inside the AlSb/InAs/InGaSb structure under a series of positive and negative voltages respectively. (c) and (d) Common logarithm of electron concentration inside the InGaSb/InAs/AlSb structure under a series of positive and negative voltages respectively. Dashed lines in (a)-(d) give the band structures under zero bias. The black arrows show the directions of EFs. Growth direction is from the left to the right.

In Fig. S5c and 5d, InGaSb/InAs/AlSb form the right half of our "W" structure. ECMI keeps increasing with rising negative voltages but first drops and then rise as positive voltage goes up, forming a "tick" shape with the monotonicity reversed around 0.25V (Fig. S5d in manuscript, red line). The similar behaviours within InGaSb/InAs/AlSb and AlSb/InAs/InGaSb suggest that the tunnelling adjustment through applying EF is feasible for the whole structure.

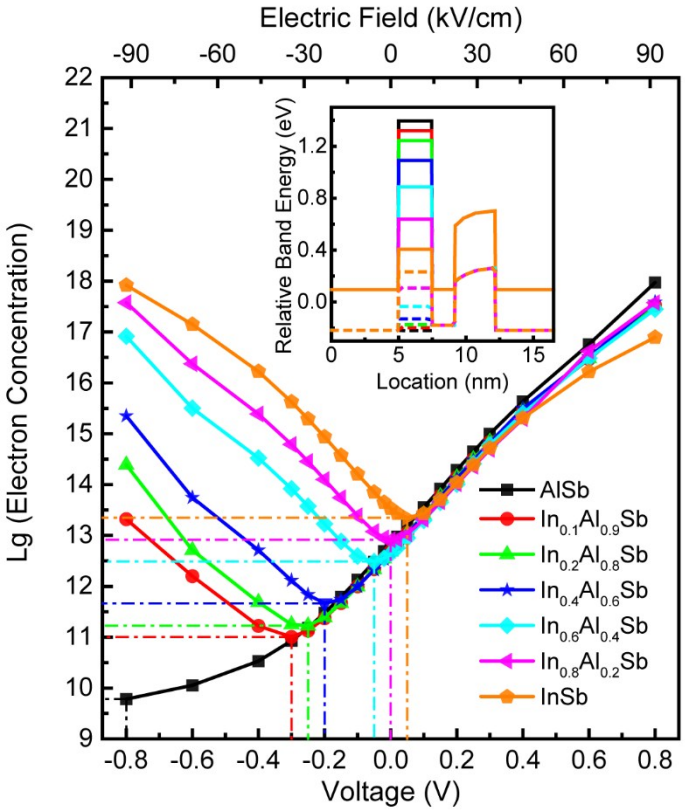

Fig. S8 Theoretical simulations of AlSb/InAs/InGaSb structure with different In content in AlSb layer. The image displays common logarithm of electron concentration under different biases at the middle point of InAs well within a series of AlSb/InAs/InGaSb models. The inset shows the different energy band alignments corresponding to seven models with different indium content in AlSb layers. The direction of EF is from the left to right for positive voltages.

This part emphasizes the variability of the initial barrier height of both AlSb and InGaSb layers and its influence on determining the location (versus voltage) and the magnitude of the minimum electron concentration. It's obvious that as indium content in the AlSb layer increases, the energy gap is narrowed with a lower CB. In the case of pure AlSb (0% content of In), the barrier height is much higher than that of InGaSb, leading to a much weaker electron tunnelling through the AlSb layer. Even if the EF of a negative voltage bends the CB of AlSb to reduce the effective barrier height and increase that of InGaSb layer at the same time, the weaker electron tunnelling intensity through AlSb compared to InGaSb still cannot be compensated. Therefore, the ECMI is dominantly determined by the electron tunnelling through InGaSb. When a positive voltage is applied, electrons are driven into the middle InAs well through InGaSb, leading to a higher ECMI. Likewise, ECMI decline as electrons escape through the InGaSb layer under negative bias. Thus, the ECMI changes

monotonically with voltages. However, as the In content in AlSb rises, the barrier height decreases and the difference in electron tunnelling intensity through AlSb and InGaSb is able to be counteracted by strong enough EF. Consequently, transition voltage of inverse monotonicity tends to be smaller with a lower CB in AlSb layer. As for a pure InSb in AlSb layer's location (100% In content), the CB is so low that the effective barrier height of InGaSb becomes larger than that of InSb. The transition voltage of inverse monotonicity becomes a positive voltage, indicating a stronger electron tunnelling intensity through InSb than InGaSb at the initial state. Moreover, one should notice that as indium content changes, the ECMI value at transition points differs. That is due to and could be adjusted by the absolute value of the effective barrier height of AlSb and InGaSb layers.

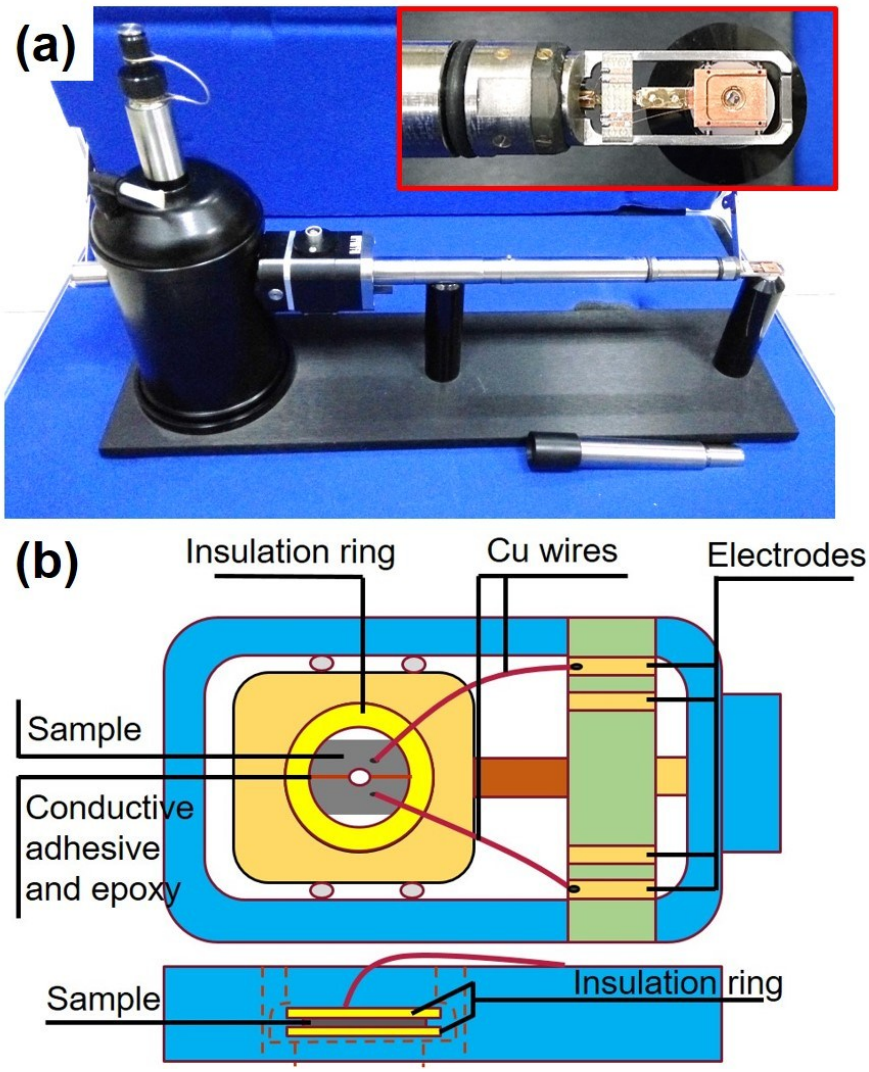

Fig. S9 Pictures and schematic diagrams of the sample holder used in our *in-situ* TEM experiments. (a) the TEM sample holder used in our experiment. The inset at the corner gives a closer view of the tip of the holder. (b) a schematic diagram of the *in-situ* bias platform shown in (a).

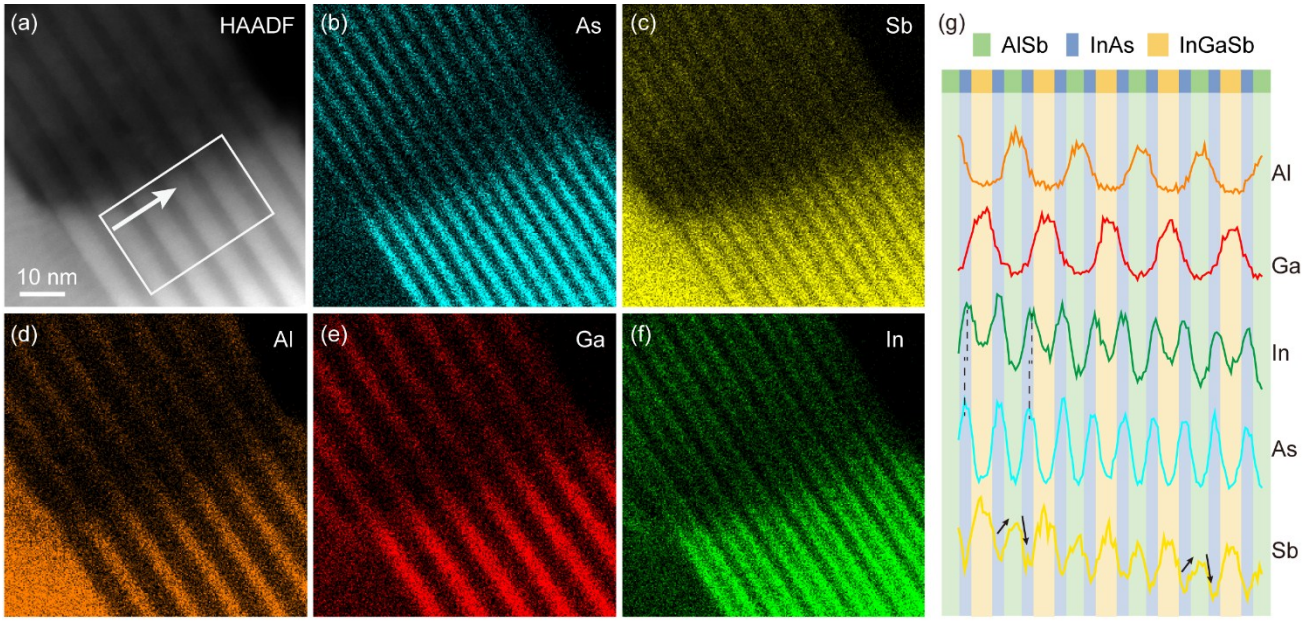

Fig. S10 Distribution of elements within the W-structure. (a) the HAADF image of the seven periods of W-structure. (b)-(f) the EDS mapping of As, Sb, Al, Ga, and In. (g) profiles of the distribution of elements. The region of the profiles is shown in the white box in (a). The colored blocks in (g) indicate the ideal locations and interfaces of the W-structure. The signals are more apparent in the bottom right part because the sample is thicker here and thinner in the top left.

In Fig. S10a, the periodic fluctuation of the image intensity refers to the seven periods of the W-structure. It's worth mentioning that both the InAs layers and the $In_{0.35}Ga_{0.65}Sb$ layers are shown as bright stripes and could almost not be distinguished in Fig. S10a due to the fact that their averaged atomic numbers are very similar (41 and 44.15 respectively, 32 for AlSb). However, their differences in composition and location are much more obvious in the EDS mapping images. Basically, all the elements contained in our system distribute regularly according to the designed structure. Meanwhile, since previous researches have indicated that the chemical segregation is ubiquitous in our material system, some characteristics of the profiles could imply its existence to some extent. For example, while As exhibits typical distribution in InAs layers, the peaks of In in InAs tend to lag slightly behind that of As. Besides, the content of Sb keeps rising during the growth of AlSb and has a steep drop when the growth of its next layer begins (shown as the black arrows in Fig. S10g). Such phenomena imply that In and Sb tend to accumulate in the growth direction. Nevertheless, the mapping is still not accurate enough to for the analysis of chemical segregation because of the spatial

resolution and the sample drift during the experiment. Therefore, GPA was selected for the analysis of the chemical deviation in the manuscript.